ONERA
THE FRENCH AEROSPACE LAB

Design and optimization of lattice structures for aerospace applications

Enrico Stragiotti

François-Xavier Irisarri[1], **Cédric Julien**[1] **and Joseph Morlier**[2]

1: ONERA - The French Aerospace Lab
DMAS - Département matériaux et structures
92320 Châtillon, France
{francois-xavier.irisarri, cedric.julien}@onera.fr

2: ICA - Institut Clément Ader
ISAE - SUPAERO
31400 Toulouse, France
joseph.morlier@isae-supaero.fr

September 15, 2023

PhD manuscript

ONERA – ISAE Supaero

Colophon

This document was typeset with the help of KOMA-Script and LaTeX using the kaobook class.

ONERA – ISAE Supaero

Contents

List of Figures

List of Tables

List of Abbreviations

DOFs	Degrees Of Freedom
HS	Hashin-Shtrikman
KS	Kreisselmeier-Steinhauser
LP	Linear Programming
MMA	Method of Moving Asymptotes

MPVCs	Mathematical Programs with Vanishing Constraints
NAND	Nested Analysis and Design
SAND	Simultaneous Analysis and Design
SIMP	Solid Isotropic Material with Penalization Method
TTO	Truss Topology Optimization

Evaluating discretization approaches for ultralight structure optimization

1

Part of the content presented in this chapter has been published and showcased during a conference as: Stragiotti, E. et al. (2021) "Towards manufactured lattice structures: a comparison between layout and topology optimization", in *AeroBest 2021 International Conference on Multidisciplinary Design Optimization of Aerospace Systems*. Book of proceedings. Lisbon, Portugal: ECCOMAS [1].

The process of topology optimization for a structure involves the selection and sizing of optimal elements within a predetermined set. As discussed in the previous chapter, in our context this set could be composed of either continuum elements (shell or volumetric) or truss-like elements. This chapter aims to assess the suitability and the inherent advantages and disadvantages of both methodologies when optimizing ultralight structures i.e. structures that exhibit an extremely low volume fraction, typically below 1%.

For this purpose, we initially establish a common optimization formulation in Section 1.1. The classic compliance minimization with volume constraint problem is reformulated as a volume minimization problem with maximum stress constraints for both discretization. Later, this framework is applied to optimize a two-dimensional test case, featuring identical dimensions, loads, and material properties. The outcomes of the comparison of both discretization approaches are presented and discussed in Section 1.2.

1.1 The formulation of a common problem: volume minimization with stress constraints

Two of the most frequently employed formulations for structural optimization are the minimization of volume while adhering to stress constraints and the minimization of compliance under volume constraints. Historically, the volume minimization formulation has been used in the first works of structural optimization of truss structures [2–4]. The problem was initially formulated in terms of member forces, ignoring the kinematic compatibility to obtain a Linear Programming (LP) problem. The formulation was modeled using the Simultaneous Analysis and Design (SAND) approach, where the equations of nodal equilibrium are treated as equality constraints, and where both nodal displacements and the cross-sectional areas of truss members serve as design variables [5].

However, to attain greater design freedom, the structure optimization field later transitioned from truss structures to continuous discretization. While truss structures offered simplicity and ease of analysis, they imposed limitations on design due to their discrete member configurations. The continuum mesh offered instead more versatility [6, 7], and has since been used for multiple different applications, e.g. the design of metamaterials [8, 9]. The SAND approach is incompatible with continuum meshes due to its excessive number of variables[1].

2. Dorn et al. (1964), 'Automatic design of optimal structures'
3. Chan (1964), 'Optimum structural design and linear programming'
4. Hemp (1973), *Optimum Structures*
5. Sankaranarayanan et al. (1994), 'Truss topology optimization with simultaneous analysis and design'
6. Bendsøe et al. (1988), 'Generating optimal topologies in structural design using a homogenization method'
7. Bendsøe (1989), 'Optimal shape design as a material distribution problem'
8. Sigmund (1994), 'Materials with prescribed constitutive parameters'
9. Zhang et al. (2006), 'Scale-related topology optimization of cellular materials and structures'

1: This preposition holds true when referring to the end of the 1980s, when computational power was scarce compared to what we have today.

Given this limitation, a new approach was required to better handle the complexity of continuum meshes.

In the Nested Analysis and Design (NAND) approach, the nodal displacement (state) variables are eliminated from the optimization problem through a process where the structural equilibrium equation is solved every iteration instead of being used as a constraint of the optimization. This results in an independent nested phase where the state equation of structural equilibrium is solved separately from the optimization algorithm. This creates a dense coupling between displacement and material density variables, necessitating a computationally expensive sensitivity analysis within the nested algorithm, typically employing the adjoint method (more information about the adjoint method on the following resurces [10, 11]). Nevertheless, if the problem is reformulated as a compliance minimization with volume constraints, the problem is self-adjoint and the adjoint algorithm is no longer necessary to evaluate the gradient sensitivities [12].

10. Tortorelli et al. (1994), 'Design sensitivity analysis'
11. Martins et al. (2021), *Engineering Design Optimization*
12. Bendsøe et al. (2004), *Topology Optimization*

However, our emphasis on operating within the aerospace sector aligns more favorably with the volume minimization problem. The choice to prioritize volume minimization in the aerospace sector is underpinned by a range of economic, environmental, and performance-related factors. It is a strategic approach that aligns with industry goals of sustainability, efficiency, and technological advancement. Additionally, as we will see later in this thesis, the volume minimization formulation will permit adding local buckling and maximum displacements constraints in an easier way. We have opted, thus, to employ the volume minimization optimization formulation for our study, and we will now review how this formulation is implemented on continuum and truss-like meshes.

1.1.1 Continuous discretization NAND minimum volume formulation

This section introduces the NAND volume minimization formulation of topology optimization for continuum meshes. We will start however presenting the more common minimum compliance formulation to explain the important notations and concepts that will be essential in developing the volume minimization formulation.

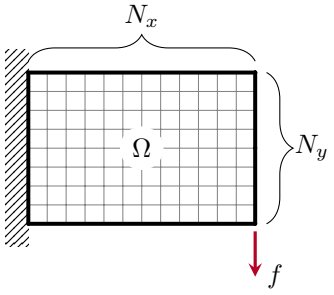

Figure 1.1: The domain Ω is discretized using $N_e = N_x N_y$ continuous 4-nodes elements.

Minimum compliance formulation Let $\Omega \in \mathbb{R}^2$ be a rectangular domain in of dimensions X and Y, containing respectively N_x and N_y linear 4-nodes elements, for a total of $N_e = N_x N_y$ elements and M nodes (see Fig. 1.1). The objective of the optimization is the minimization of the compliance C of the structure, equivalent to finding the structure with the least possible nodal displacement with respect to a defined set of boundary conditions. The problem $\mathbb{T}_0$ is

stated in terms of the design variables $\boldsymbol{\rho}$ as follows:

$$\begin{aligned} \min_{\boldsymbol{\rho}} \quad & C = \sum_i \boldsymbol{u}_{e,i}^T \boldsymbol{K}_{e,i} \boldsymbol{u}_{e,i} = \boldsymbol{f}^T \boldsymbol{u} && \forall i \in [0, \dots, N_e] \\ \text{s.t.} \quad & \frac{\sum_i \left(\overline{\widetilde{\rho}}_i v_i\right) / V_0}{V^*} - 1 \leq 0 && \forall i \in [0, \dots, N_e] \qquad (\mathbb{T}_0) \\ & \boldsymbol{K}\boldsymbol{u} = \boldsymbol{f} \\ & 0 \leq \rho_i \leq 1. && \forall i \in [0, \dots, N_e] \end{aligned}$$

The design variables $\boldsymbol{\rho}$ are defined for every element of the structure as $\boldsymbol{\rho} = [\rho_1, \rho_2, \dots, \rho_{Ne}]^T$, with $\rho_i \in [0, 1]$, $\forall i \in [0, \dots, N_e]$. The physical densities $\overline{\widetilde{\boldsymbol{\rho}}}$ are related to design variables through density filtering and threshold projection [13], as explained later in the document. V^* is the prescribed volume fraction that acts as constraint of the minimization problem, while v_i represents the area of the i-th element and V_0 the total area of the domain Ω. $\boldsymbol{K}\boldsymbol{u} = \boldsymbol{f}$ is the state equation of the problem and defines the elastic response of the structure to an external nodal load $\boldsymbol{f} = [f_1, f_2, \dots, f_{2M}]^T$. The global stiffness matrix $\boldsymbol{K}$ is assembled from the element stiffness matrix $\boldsymbol{K} = \sum_{i \in \Omega} \boldsymbol{K}_{e,i}$ and $\boldsymbol{K}_{e,i} = E_i \boldsymbol{K}_{e,0}$ where $\boldsymbol{K}_{e,0}$ represents the element stiffness matrix relative to the chosen type of element (linear or quadratic) and $E_i(\overline{\widetilde{\rho}}_i)$ the Young's modulus of the i-th element.

13. Wang et al. (2011), 'On projection methods, convergence and robust formulations in topology optimization'

The material scheme used to interpolate between void and full material is the well known Solid Isotropic Material with Penalization Method (SIMP) [7, 14] approach. It is governed by the equation:

$$E_i(\overline{\widetilde{\rho}}_i) = E_{\min} + \overline{\widetilde{\rho}}_i^p (E_0 - E_{\min}), \tag{1.1}$$

where the parameter p penalizes the intermediate densities and pushes the result to a black and white result. E_0 is the Young's modulus of the dense material and $E_{\min}$ is a small value used to avoid the global stiffness matrix $\boldsymbol{K}$ from being singular when $\overline{\widetilde{\rho}}_i = 0$.

7. Bendsøe (1989), 'Optimal shape design as a material distribution problem'

14. Bendsøe et al. (1999), 'Material interpolation schemes in topology optimization'

In this study we set these parameters to $E_0 = 1$, and $E_{\min} = 10^{-9}$. The value of the penalization parameter p is selected as $p = 3$ because in that way the intermediate densities respect the Hashin-Shtrikman (HS) bounds [14, 15]. This describes the boundaries of attainable isotropic material characteristics when dealing with composites (materials with microscopic structures) using two specified, linearly elastic, isotropic materials (in our case the solid and the empty phases).

15. Hashin et al. (1963), 'A variational approach to the theory of the elastic behaviour of multiphase materials'

Spatial filtering and projection Multiple approaches have been developed to solve the problems linked to the mesh discretization, such as mesh dependence or the checkerboard problem [16]. Filtering the sensitivity information of the optimization problem proved to be an effective approach to guarantee independence from mesh

16. Díaz et al. (1995), 'Checkerboard patterns in layout optimization'

17. Sigmund (1994), 'Design of Material Structures using Topology Optimization'

18. Sigmund (1997), 'On the Design of Compliant Mechanisms Using Topology Optimization'

resolution [17, 18]. In the present research we decided instead to directly filter the density field $\boldsymbol{\rho}$ using the 2D convolution operator [19]. The weight function w (or kernel) of the convolution is defined as:

19. Sigmund (2007), 'Morphology-based black and white filters for topology optimization'

$$w(d_j) = R - d_j, \quad j \in \mathbb{N}_{i,R} \tag{1.2}$$

where $\mathbb{N}_{i,R}$ represent the set of elements lying within a circle of radius R centered on the i-th element and d_j is the distance of the j-th element to the center of the filter (see Fig. 1.2).

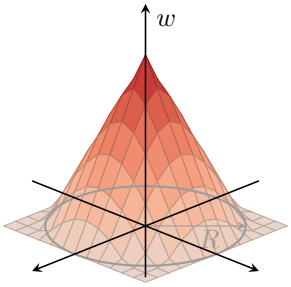

Figure 1.2: Kernel of the 2D convolution operator.

The filtered values of the design variable calculated as:

$$\widetilde{\rho}_i = \frac{\sum_{j\in\mathbb{N}_{i,R}} w(d_j)v_j\rho_j}{\sum_{j\in\mathbb{N}_{i,R}} w(d_j)v_j}. \tag{1.3}$$

As the filtering phase produces a large quantity of gray elements, a smooth projection technique based on the *tanh* function is implemented [13]:

13. Wang et al. (2011), 'On projection methods, convergence and robust formulations in topology optimization'

$$\overline{\widetilde{\rho}}_j = \frac{\tanh(\beta\eta) + \tanh(\beta(\widetilde{\rho}_j - \eta))}{\tanh(\beta\eta) + \tanh(\beta(1-\eta))}, \tag{1.4}$$

where β is a parameter that define the slope of this approximation function: the larger the value of β, the less intermediate elements are present in the structure topology. η is the threshold value of the projection. Using Equation 1.4 is not volume conservative for all values of η, and to stay conservative we use a volume-increasing filter [20]. The value of $\eta = 0.4$ is then chosen.

20. Ferrari et al. (2020), 'A new generation 99 line Matlab code for compliance topology optimization and its extension to 3D'

The derivative of the filtered density $\widetilde{\boldsymbol{\rho}}$ with respect to the design variable $\boldsymbol{\rho}$ is written deriving Equation 1.3:

$$\frac{\partial\widetilde{\rho}_i}{\partial\rho_j} = \frac{w(d_j)v_j}{\sum_{j\in\mathbb{N}_{i,R}} w(d_j)v_j}. \tag{1.5}$$

The sensitivity of the physical densities $\overline{\widetilde{\boldsymbol{\rho}}}$ with respect to the filtered $\widetilde{\boldsymbol{\rho}}$ can be written as:

$$\frac{\partial\overline{\widetilde{\rho}}_j}{\partial\widetilde{\rho}_j} = \beta\frac{1 - \tanh^2(\beta(\widetilde{\rho}_j - \eta))}{\tanh(\beta\eta) + \tanh(\beta(1-\eta))}. \tag{1.6}$$

Using the chain rule it is possible to write:

$$\frac{\partial h}{\partial\rho_i} = \sum_{j\in\mathbb{N}_{i,R}} \frac{\partial f}{\partial\overline{\widetilde{\rho}}_j}\frac{\partial\overline{\widetilde{\rho}}_j}{\partial\widetilde{\rho}_j}\frac{\partial\widetilde{\rho}_j}{\partial\rho_i}, \tag{1.7}$$

where h represents a generic function.

Objective and constraint funtions Up until this point, we have been focused on the compliance minimization formulation $\mathbb{T}_0$. Moving

forward, we introduce the necessary modifications to transition into the volume minimization formulation with stress constraints. This formulation will be used to compare the continuous mesh with truss-link structure optimization.

The objective of the optimization is to minimize the volume of a structure subject to a specified load case. The volume of the structure V is expressed in percentage with respect to the total volume V_0 of the domain Ω:

$$V = \frac{1}{V_0} \sum_{i \in \Omega} \overline{\widetilde{\rho}}_i v_i, \tag{1.8}$$

where v_i is the elementary volume occupied by the i-th element. In this thesis, we assume that v_i is equal for all the elements, and thus Equation 1.8 is simplified as follows:

$$V = \frac{1}{N_e} \sum_{i \in \Omega} \overline{\widetilde{\rho}}_i. \tag{1.9}$$

The normalized local stress constraint $\boldsymbol{g}_{\text{st}}$ are formulated as:

$$\frac{\sigma_{\text{VM},j}}{\sigma_L} - 1 \leq 0, \quad \forall j \in \Omega_{mat}(\boldsymbol{\rho}) \tag{g_{st}}$$

where $\Omega_{mat}(\boldsymbol{\rho}) \subseteq \Omega$ represents the design-dependent set of elements with a non-zero density, $\sigma_{\text{VM},j}$ is the equivalent von Mises stress for the j-th element, and σ_L is the maximum allowable of the material.

A first difficulty that arises is that the stress constraints are defined only for the elements where $\overline{\widetilde{\rho}}_i > 0$, while $\overline{\widetilde{\rho}}_i \in [0, 1]$. Thus, the set of constraints changes during the optimization. This class of problems are called Mathematical Programs with Vanishing Constraints (MPVCs) [21] and are known for being difficult to solve with a gradient descent optimization algorithm. The original set of constraints $\boldsymbol{g}_{\text{st}}$ is then reformulated into an equivalent design-independent set of constraints $\bar{\boldsymbol{g}}_{\text{st}}$ as follows [22]:

$$\overline{\widetilde{\rho}}_i \left(\frac{\sigma_{\text{VM},i}}{\sigma_L} - 1 \right) \leq 0, \quad \forall i \in \Omega. \tag{$\bar{g}_{\text{st}}$}$$

21. Achtziger et al. (2008), 'Mathematical programs with vanishing constraints'

22. Cheng et al. (1992), 'Study on Topology Optimization with Stress Constraints'

Von Mises stress evaluation The evaluation of the equivalent stress of an element follows the formulation proposed by Von Mises. Let us take a four-nodes quadrilateral linear element with a single integration (or Gauss) point in the center and four $2a$ equal-length sides (see Fig. 1.3). If bilinear shape function are used to interpolate the displacement field, we can evaluate the deformations at the integration

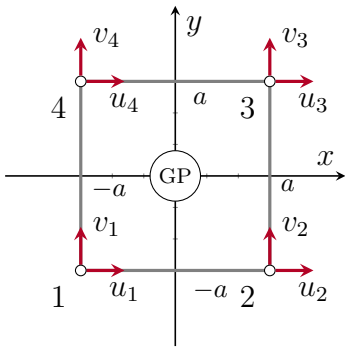

Figure 1.3: A four-node quadrilateral element. GP is the Gaussian integration point for which the equivalent stress is evaluated.

point as:

$$\begin{pmatrix}\varepsilon_x\\ \varepsilon_y\\ \gamma_{xy}\end{pmatrix} = \boldsymbol{B}_s \boldsymbol{q}_s, \text{ with } \boldsymbol{B}_s = \frac{1}{4a}\begin{pmatrix}-1 & 1 & 1 & -1 & 0 & 0 & 0 & 0\\ 0 & 0 & 0 & 0 & -1 & -1 & 1 & 1\\ -1 & -1 & 1 & 1 & -1 & 1 & 1 & -1\end{pmatrix}, \tag{1.10}$$

where $\boldsymbol{q}_s = (u_1, u_2, u_3, u_4, v_1, v_2, v_3, v_4)^T$ represents the vector of the displacement degrees of freedom of the element.

The stress tensor is evaluated using the elasticity Hooke's law in 2D as follows:

$$\begin{pmatrix}\sigma_x\\ \sigma_y\\ \tau_{xy}\end{pmatrix} = \boldsymbol{C}_e \begin{pmatrix}\varepsilon_x\\ \varepsilon_y\\ \gamma_{xy}\end{pmatrix} \quad \text{with} \quad \boldsymbol{C}_e = \frac{E}{1-\nu^2}\begin{pmatrix}1 & \nu & 0\\ \nu & 1 & 0\\ 0 & 0 & G\end{pmatrix}. \tag{1.11}$$

The equivalent Von Mises stress of the element can then be written as:

$$\langle \boldsymbol{\sigma}_{\text{VM}} \rangle = \sqrt{\sigma_x^2 + \sigma_y^2 - \sigma_x\sigma_y + 3\tau_{xy}} \tag{1.12}$$

$$= \sqrt{\begin{pmatrix}\sigma_x & \sigma_y & \tau_{xy}\end{pmatrix}\begin{pmatrix}1 & -1/2 & 0\\ -1/2 & 1 & 0\\ 0 & 0 & 3\end{pmatrix}\begin{pmatrix}\sigma_x\\ \sigma_y\\ \tau_{xy}\end{pmatrix}} \tag{1.13}$$

$$= \sqrt{\boldsymbol{q}_s^T \boldsymbol{B}_s^T \boldsymbol{C}_e^T \boldsymbol{D}_{\text{VM}} \boldsymbol{C}_e \boldsymbol{B}_s \boldsymbol{q}_s}, \text{ with } \boldsymbol{D}_{\text{VM}} = \begin{pmatrix}1 & -1/2 & 0\\ -1/2 & 1 & 0\\ 0 & 0 & 3\end{pmatrix} \tag{1.14}$$

$$\langle \boldsymbol{\sigma}_{\text{VM}} \rangle = \sqrt{\boldsymbol{q}_s^T \boldsymbol{S} \boldsymbol{q}_s}, \quad \text{with } \boldsymbol{S} = \boldsymbol{B}_s^T \boldsymbol{C}_e^T \boldsymbol{D}_{\text{VM}} \boldsymbol{C}_e \boldsymbol{B}_s \tag{1.15}$$

Microscopic and macroscopic stress In stress-constrained topology optimization the element stress is usually evaluated using the microscopic stress formulation, assuming that there is no direct correlation between stress and density [23]. Indeed, the use of the macroscopic stress in volume minimization optimization problems creates all-void design [24]. The properties that the microscopic stress should present are:

(i) The stress criterion should be mathematically as simple as possible, as the relationship between Young's modulus and density. This permits a simple numerical implementation.
(ii) To mimic the real physical behavior, the microscopic stress should be inversely proportional to density.
(iii) The microscopic stress should converge to a non-zero value at zero density. This requisite is deduced from investigations into the asymptotic stress behavior in thin layers [25].

23. Duysinx et al. (1998), 'Topology optimization of continuum structures with local stress constraints'
24. Le et al. (2010), 'Stress-based topology optimization for continua'
25. Verbart et al. (2017), 'A unified aggregation and relaxation approach for stress-constrained topology optimization'

The relation within stress and displacement is written as:

$$\langle \sigma_{\text{VM}} \rangle = \boldsymbol{C}_e(\langle E \rangle)\langle \boldsymbol{\varepsilon} \rangle \tag{1.16}$$

where the variables between angular brackets $\langle \dots \rangle$ represent macroscopic variables.

Combining (i) and (ii) with Equations 1.1, and 1.16, the microscopic stress can be written as:

$$\boldsymbol{\sigma}_{\text{VM}} = \frac{\langle \boldsymbol{\sigma}_{\text{VM}} \rangle}{\rho_e^q} = \rho_e^{p-q} \boldsymbol{C}_e(E_0)\langle \boldsymbol{\varepsilon} \rangle \tag{1.17}$$

where the exponent q is a number greater than 1.

One possible choice that satisfy all the requirements is $q = p$ [24–27]. Thus, the microscopic stress is defined as:

$$\boldsymbol{\sigma}_{\text{VM}} = \boldsymbol{C}_e(E_0)\langle \boldsymbol{\varepsilon} \rangle \tag{1.18}$$

From a physical perspective, the significance of microscopic stress becomes evident when considering an element with intermediate density and a porous microstructure. The microscopic stress presented in Equation 1.18 measures the stress of the microstructure. It is grounded in the assumption that the macroscopic deformations of the homogenized element generate within the microstructure of the element a stress state that remains unaffected by the density of the element itself.

24. Le et al. (2010), 'Stress-based topology optimization for continua'
25. Verbart et al. (2017), 'A unified aggregation and relaxation approach for stress-constrained topology optimization'
26. Holmberg et al. (2013), 'Stress constrained topology optimization'
27. Silva et al. (2019), 'Stress-constrained topology optimization considering uniform manufacturing uncertainties'

Constraints aggregation and relaxation When optimizing a structure with stress constraints using a NAND formulation, two primary challenges commonly arise:

(i) Is it known in the literature [28, 29] that stress-based topolgy optimization suffer from the *singular minima* (or *singularity*) problem: firstly observed on truss structure optimization [30], these *minima* are almost inaccessible to standard gradient-based optimizer, and they represent the *minima* of the optimization. This because achieving the optimal solution to a problem using continuous design variables may necessitate passing through a state where the optimization constraints are violated, i.e. the *minimum* is on a lower dimension compared to the design space. This problem is often solved using a technique called *constraints relaxation* [31].

(ii) The stress is a local measure, and thus a large set of constraints is generated when a reasonably fine mesh is used (one element, one constraint). This problem is often solved using a technique called *constraints aggregation* or *global constraints* [32].

Following the work developed by Verbart *et al.* [25], the lower bound

31. Cheng et al. (1997), 'ε-relaxed approach in structural topology optimization'
32. Silva et al. (2021), 'Local versus global stress constraint strategies in topology optimization'
25. Verbart et al. (2017), 'A unified aggregation and relaxation approach for stress-constrained topology optimization'

33. Kreisselmeier et al. (1979), 'Systematic Control Design by Optimizing a Vector Performance Index'

Kreisselmeier-Steinhauser (KS) function [33] is used to approximate the local relaxed stress constraint maximum. The authors discovered that employing lower-bound KS aggregation functions to approximate the maximum operator in stress-constrained topology optimization eliminates the need for stress constraint relaxation methods to address the singularity issue. This is because the lower-bound functions inherently offer a combined effect of constraints aggregation and relaxation. The KS aggregated stress constraint function is defined as follows:

$$G_{\mathrm{KS}}^{\mathrm{L}} = \frac{1}{P} \ln \left(\frac{1}{N_e} \sum e^{P \bar{g}_i} \right). \tag{1.19}$$

Its main advantage over other different formulations is that it uses a single hyperparameter P to control the aggregation and the relaxation of the constraints simultaneously.

Minimum volume formulation The NAND minimum volume formulation for continuous discretization is written Equations 1.9, and 1.19 as:

$$\begin{aligned} \min_{\rho} \quad & V = \frac{1}{N_e} \sum_{i \in \Omega} \overline{\widetilde{\rho}}_i, \\ \text{s.t.} \quad & G_{\mathrm{KS}}^{\mathrm{L}} = \frac{1}{P} \ln \left(\frac{1}{N_e} \sum_{i \in \Omega} e^{P \bar{g}_i} \right) \leq 0 \\ & \boldsymbol{K}\boldsymbol{u} = \boldsymbol{F} \\ & 0 \leq \rho_i \leq 1, \end{aligned} \tag{$\mathbb{T}_1$}$$

The optimization is carried out using a gradient descent optimization algorithm for which the sensitivities are given in analytical form. Using analytic gradients is in general more efficient than finite differences as it avoids the need for multiple function evaluations, making the optimization process faster and more precise.

Sensitivity analysis of the objective function The objective of this section is to quickly present the calculation of the analytical sensitivity of the volume with respect to the design variable ρ. Deriving Equation 1.9 we obtain:

$$\frac{\partial V}{\partial \overline{\widetilde{\rho}}_i} = \frac{1}{N_e}. \tag{1.20}$$

The sensitivity of the objective function can then be evaluated using Equations 1.20, 1.5, 1.6, and 1.7 as follows:

$$\frac{dV}{d\rho_i} = \sum_{j \in \mathbb{N}_{i,R}} \frac{\partial V}{\partial \overline{\widetilde{\rho}}_j} \frac{\partial \overline{\widetilde{\rho}}_j}{\partial \widetilde{\rho}_j} \frac{\partial \widetilde{\rho}_j}{\partial \rho_i}. \tag{1.21}$$

Sensitivity analysis of the constraint function This section focuses on the details of the calculation of how the constraint function $G^{\mathrm{L}}_{\mathrm{KS}}$ changes with respect to the design variable $\boldsymbol{\rho}$.

As the constraint function $G^{\mathrm{L}}_{\mathrm{KS}} = G(\overline{\overline{\boldsymbol{\rho}}}, \boldsymbol{u}(\overline{\overline{\boldsymbol{\rho}}}))$ is explicitly and implicitly (via the relationship with $\boldsymbol{u}$) depending on $\overline{\overline{\boldsymbol{\rho}}}$, the first-order derivative is evaluated using the total derivative formula:

$$\frac{\partial G^{\mathrm{L}}_{\mathrm{KS}}}{\partial \overline{\overline{\rho}}_j} = \frac{dG}{d\overline{\overline{\rho}}_j} = \frac{\partial G}{\partial \overline{\overline{\rho}}_j} + \frac{\partial G}{\partial \boldsymbol{u}} \frac{d\boldsymbol{u}}{d\overline{\overline{\rho}}_j} \tag{1.22}$$

As function $G^{\mathrm{L}}_{\mathrm{KS}}$ depends on $\boldsymbol{u}$ via the stresses σ_i, it is possible to write:

$$\frac{\partial G}{\partial \boldsymbol{u}} = \sum_{i \in \Omega} \left(\frac{\partial G}{\partial \sigma_i} \frac{\partial \sigma_i}{\partial \boldsymbol{u}} \right) \tag{1.23}$$

Combining Eq. 1.22 with Eq. 1.23, we obtain:

$$\frac{dG}{d\overline{\overline{\rho}}_j} = \underbrace{\frac{\partial G}{\partial \overline{\overline{\rho}}_j}}_{A} + \sum_{i \in \Omega} \left(\underbrace{\frac{\partial G}{\partial \sigma_i}}_{B} \underbrace{\frac{\partial \sigma_i}{\partial \boldsymbol{u}}}_{C} \right) \underbrace{\frac{d\boldsymbol{u}}{d\overline{\overline{\rho}}_j}}_{D} \tag{1.24}$$

We compute the four factors separately:

A – The first term represents the explicit relationship of G to the physical densities and its calculation is straightforward:

$$\frac{\partial G}{\partial \overline{\overline{\rho}}_j} = \frac{1}{P} \frac{\left(\frac{\sigma_{\mathrm{VM},j}}{\sigma_L} - 1 \right) \frac{1}{N_e} P e^{P \bar{g}_j}}{\frac{1}{N_e} \sum_k e^{P \bar{g}_k}} = \left(\frac{\sigma_{\mathrm{VM},j}}{\sigma_L} - 1 \right) \frac{e^{P \bar{g}_j}}{\sum_k e^{P \bar{g}_k}} \tag{1.25}$$

B – The second term can be calculated using the chain rule:

$$\frac{\partial G}{\partial \sigma_i} = \frac{\partial G}{\partial \bar{g}_i} \frac{\partial \bar{g}_i}{\partial \sigma_i} = \frac{1}{P} \frac{\frac{1}{N_e} P e^{P \bar{g}_i}}{\frac{1}{N_e} \sum_k e^{P \bar{g}_k}} \frac{\overline{\overline{\rho}}_i}{\sigma_L} = \frac{\overline{\overline{\rho}}_i}{\sigma_L} \frac{e^{P \bar{g}_i}}{\sum_k e^{P \bar{g}_k}} \tag{1.26}$$

C – We reformulate Eq. 1.15 to be written in global coordinates instead of local:

$$\sigma_i^2 = \boldsymbol{q}_s^T \boldsymbol{S} \boldsymbol{q}_s = \boldsymbol{u}^T |\boldsymbol{S_i}|_g \boldsymbol{u} \tag{1.27}$$

where $|\boldsymbol{S_i}|_g$ represents the matrix $\boldsymbol{S}$ of Equation 1.15written on global coordinates [2]. We can now differentiate Equation 1.27 with respect of the displacement field in global coordinates $\boldsymbol{u}$ to obtain:

$$\frac{\partial \sigma_i}{\partial \boldsymbol{u}} = \frac{|\boldsymbol{S_i}|_g \boldsymbol{u}}{\sigma_i} \tag{1.28}$$

Equations 1.26, and 1.28 are now combined to obtain the result

2: The matrix $|\boldsymbol{S_i}|_g$ can be calculated using the very same assmebling approach used for the stiffness matrix $\boldsymbol{K}$ starting from the elemental stiffness matrix $\boldsymbol{K}_e$. As the global stiffness matrix $\boldsymbol{K}$, $|\boldsymbol{S_i}|_g$ is symmetric and sparse.

of the product of the **B** and **C** terms. As a result, the derivatives of G with respect to $\boldsymbol{u}$, are written as:

$$\frac{\partial G}{\partial \boldsymbol{u}} = \frac{\frac{\bar{\bar{\rho}}_j}{\sigma_L \sigma_j} e^{P\tilde{g}_i}}{\sum_i e^{P\tilde{g}_i}} |\boldsymbol{S}_j|_g \boldsymbol{u} \tag{1.29}$$

D – To calculate the last term, we take the static equilibrium equation $\boldsymbol{K}\boldsymbol{u} = \boldsymbol{f}$ and differentiating it with respect to the physical densities $\bar{\bar{\rho}}_j$, obtaining:

$$\frac{\partial \boldsymbol{K}}{\partial \bar{\bar{\rho}}_j}\boldsymbol{u} + \boldsymbol{K}\frac{\partial \boldsymbol{u}}{\partial \bar{\bar{\rho}}_j} = 0 \iff \frac{\partial \boldsymbol{u}}{\partial \bar{\bar{\rho}}_j} = -\boldsymbol{K}^{-1}\frac{\partial \boldsymbol{K}}{\partial \bar{\bar{\rho}}_j}\boldsymbol{u}, \tag{1.30}$$

where

$$\frac{\partial \boldsymbol{K}}{\partial \bar{\bar{\rho}}_j} = (E_0 - E_{\min}) p \bar{\bar{\rho}}_j^{p-1} \boldsymbol{K}_{e,j}. \tag{1.31}$$

Equation 1.31 represent the well known first-derivative term of the global stiffness matrix $\boldsymbol{K}$ with respect of the physical densities $\bar{\bar{\rho}}_j$ when using SIMP material scheme [12]. We finally obtain the last term:

12. Bendsøe et al. (2004), *Topology Optimization*

$$\frac{d\boldsymbol{u}}{d\bar{\bar{\rho}}_j} = -\boldsymbol{K}^{-1}\left((E_0 - E_{\min}) p \bar{\bar{\rho}}_j^{p-1} \boldsymbol{K}_e\right)\boldsymbol{u} \tag{1.32}$$

Combining Eq. 1.24, Eq. 1.25, Eq. 1.29, and Eq. 1.32, we finally obtain:

$$\frac{\partial G_{\text{KS}}^{\text{L}}}{\partial \bar{\bar{\rho}}_j} = \left(\frac{\sigma_{\text{VM},j}}{\sigma_L} - 1\right)\frac{e^{P\tilde{g}_j}}{\sum_k e^{P\tilde{g}_k}} - \boldsymbol{K}^{-1}\frac{\partial G}{\partial \boldsymbol{u}}\left(\frac{\partial \boldsymbol{K}}{\partial \bar{\bar{\rho}}_j}\right)\boldsymbol{u} \tag{1.33}$$

3: More information about the adjoint method used to analytically calculate the first-order derivatives can be found on the Martins *et al.* book [11].

To avoid the explicit calculation of $\boldsymbol{K}^{-1}$ we use the *adjoint method*[3]. Here is the linear system that, once solved, permits to calculate $\boldsymbol{\psi}$:

$$\boldsymbol{K}\boldsymbol{\psi} = \frac{\partial G}{\partial \boldsymbol{u}} \iff \boldsymbol{\psi} = \boldsymbol{K}^{-1}\frac{\partial G}{\partial \boldsymbol{u}} \tag{1.34}$$

This formula is called *adjoint equation*. This equation is solved for $\boldsymbol{\psi}$ and the result used to evaluate:

$$\frac{\partial G_{\text{KS}}^{\text{L}}}{\partial \bar{\bar{\rho}}_j} = \left(\frac{\sigma_{\text{VM},j}}{\sigma_L} - 1\right)\frac{e^{P\tilde{g}_j}}{\sum_k e^{P\tilde{g}_k}} - \boldsymbol{\psi}\left(\frac{\partial \boldsymbol{K}}{\partial \bar{\bar{\rho}}_j}\right)\boldsymbol{u} \tag{1.35}$$

Solving linear system 1.34 instead of directly calculating the inverse matrix of $\boldsymbol{K}$ is more efficient from a performance perspective. The cost of solving a system using the Cholesky decomposition is $\mathcal{O}(N^3/3)$, while a matrix inversion is $\mathcal{O}(N^3)$.

where N represents the size of the square matrix describing the linear system. Equation 1.35 represents the first-order derivative equation used to evaluate the sensitivity of the constraint function G_{KS}^{L} with respect to the physical densities $\bar{\bar{\rho}}$. The value of $\boldsymbol{\psi}$ is calculated every iteration solving the linear system 1.34.

The sensitivity of the aggregated contraint function with respect to the design variable $\boldsymbol{\rho}$ is evaluated using Equations 1.20, 1.5, 1.6, and 1.7 as follows:

$$\frac{dG^{\mathrm{L}}_{\mathrm{KS}}}{d\rho_i} = \sum_{j \in \mathbb{N}_{i,R}} \frac{\partial G^{\mathrm{L}}_{\mathrm{KS}}}{\partial \overline{\widetilde{\rho}}_j} \frac{\partial \overline{\widetilde{\rho}}_j}{\partial \widetilde{\rho}_j} \frac{\partial \widetilde{\rho}_j}{\partial \rho_i}. \tag{1.36}$$

1.1.2 Truss discretization SAND minimum volume formulation

We are now shifting our focus from continuous structures to discrete truss systems, describing the Truss Topology Optimization (TTO) (also knows in early literature as layout optimization), a structure optimization method that focuses on discrete structures. In his most used formulation, TTO aims at reducing material usage while meeting stress criteria using a SAND approach. The problem is already well-posed for the comparison with continuous discretization, and our intention is to now explore specific key concepts within its established framework.

Classical Michell structures The characteristics of these structures are described by some simple criteria that date to the end of the 19th and the beginning of the 20th century. When a structure is statically determinate — i.e. the structure is not a mechanism, and it is not over-constrained by the supports — the Maxwell theorem [34] states that:

$$\sum_{\forall i | q_i > 0} \ell_i q_i + \sum_{\forall i | q_i < 0} \ell_i q_i = \text{const.} \tag{1.37}$$

34. Maxwell (1870), 'I.—On Reciprocal Figures, Frames, and Diagrams of Forces'

where ℓ_i and q_i represent the length and the axial force of the i-th member, respectively. The constant value at the right of Equation 1.37 depends on the nature of the boundary conditions and the material used. The Maxwell theorem dictates that any increment in compression forces must be counterbalanced by an equivalent increase in tension forces when the structure remains topologically unchanged. So for statically determinate structures the structure layout is not influenced by the ratio between σ_c and σ_t, the Young's modulus E of the material, nor the force magnitude.

Starting from Maxwell's findings, Michell theorized two further criteria for optimal truss structures [35] valid when the maximum allowable stress is equal in tension and compression ($\sigma_t = \sigma_c$) and when the supports of the structure are statically determinate. The first one states that all the members of an optimal structure should present internal stress equal in magnitude to the maximum allowable value of the material - i.e. the structure is *fully stressed*. The second criterion asserts that the strain of all the members of the structure should be equal and there should be no other point having a strain higher than this value. As formulated, these two criteria are known as the Michell criteria. The second criterion was later generalized by Hemp [4] as:

35. Michell (1904), 'The limits of economy of material in frame-structures'

4. Hemp (1973), *Optimum Structures*

$$-\frac{1}{\sigma_c} \leq \varepsilon \leq \frac{1}{\sigma_t} \tag{1.38}$$

Compared to the second Michell criterion, Equation 1.38 permits to correctly identify the minimum volume structure even when different strength values for compression and tension and different support types are taken. These criteria are known as the Michell-Hemp criteria.

Plastic material formulation The rigid-plastic formulation characterizes the material as entirely rigid up to the point of reaching the yield stress, denoted as σ_y, and subsequently assumes a constant stress level of σ_y once that threshold is exceeded. This formulation is a clear consequence of the application of the Michell-Hemp criteria and has thus been used in the very first work of layout optimization (also known as TTO) [2–4].

2. Dorn et al. (1964), 'Automatic design of optimal structures'
3. Chan (1964), 'Optimum structural design and linear programming'
4. Hemp (1973), *Optimum Structures*

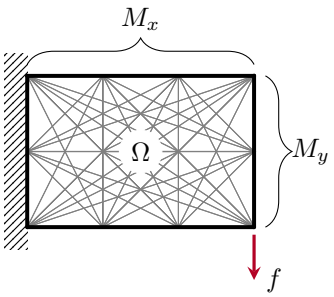

Figure 1.4: The domain Ω is discretized using a set of straight members connecting a set of nodes. THis framework is known as ground structure.

The ground structure approach The ground structure is a framework composed of various structural members that connect specified points or nodes in two- or three-dimensional space (see Fig. 1.4). These members can take the form of beams, columns, wires, or bars elements, depending on the specific structural requirements. In this thesis we will deal with trusses, and so the chosen element is the bar. Since the nodes within the ground structure are considered pin-joints, all straight members exclusively face either tension or compression loads.

Depending on how the connectivity of the grid of nodes is, we can experience very different ground structures. In a fully connected ground structure, every node within the system is linked to every other node, resulting in a dense and redundant structural configuration. The number of bars N_{el} of a fully connected ground structure can be determined using the following formula:

$$N_{el} = \frac{M \cdot (M-1)}{2} \tag{1.39}$$

where M represent the number of nodes of the structure.

In classic works, the ground structure is used as the start of the optimization, where the optimized structure is obtained as a subset of the initial ground structure, but multiple alternative approaches have been proposed since then, e.g. starting from a very coarse ground structure that is enriched during the analysis [36], or giving the nodes of a coarse ground structure the possibility to move, during [37–39], or after the optimization, simultaneously reducing the number of active members of the solution [40, 41].

36. Gilbert et al. (2003), 'Layout optimization of large-scale pin-jointed frames'
37. Pedersen (1973), 'Optimal Joint Positions for Space Trusses'
38. Achtziger (2007), 'On simultaneous optimization of truss geometry and topology'
39. Descamps et al. (2013), 'A lower-bound formulation for the geometry and topology optimization of truss structures under multiple loading'
40. He et al. (2015), 'Rationalization of trusses generated via layout optimization'
41. Lu et al. (2023), 'Reducing the number of different members in truss layout optimization'

Optimization formulation The volume minimization formulation with maximum stress constraints is stated in terms of members' cross-sectional areas $\boldsymbol{a}$ and member forces $\boldsymbol{q}$ as follows:

$$\begin{aligned} \min_{\boldsymbol{a},\boldsymbol{q}} \quad & V = \boldsymbol{\ell}^T \boldsymbol{a} && \text{(Volume)} \\ \text{s.t.} \quad & \boldsymbol{B}_s \boldsymbol{q} = \boldsymbol{f} && \text{(Force equilibrium)} \\ & -\sigma_c \boldsymbol{a} \leq \boldsymbol{q} \leq \sigma_t \boldsymbol{a} && \text{(Stress constraints)} \\ & \boldsymbol{a} \geq 0, \end{aligned} \qquad (\mathbb{P}_0)$$

where $\boldsymbol{B}_s$ is a $N_{\text{dof}} \times N_{\text{el}}$ matrix containing the direction cosines of the j-th member with respect to the i-th degree of freedom to calculate the nodal force equilibrium, and where N_{dof} is the number of Degrees Of Freedom (DOFs), equal to $2M$ or $3M$ for a two- or a three-dimensional load case, respectively. $\boldsymbol{q} = [q_1, q_2, \ldots, q_{N_{\text{el}}}]^T$ is the vector containing the internal member forces, with a positive sign when in tension, caused by the external load $\boldsymbol{f} = [f_1, f_2, \ldots, f_{N_{\text{dof}}}]^T$. The state variable $\boldsymbol{a} = [a_1, a_2, \ldots, a_{N_{\text{el}}}]^T$ represents the cross-sectional area of the N_{el} members of the structure. σ_c and σ_t are the compressive and tensile maximum allowable stresses of the material, respectively. This formulation takes into account only the linear behavior of the structure and is equivalent to the original and well-studied member force formulation [2, 12].

The resolution of Problem $\mathbb{P}_0$ frequently produces complex structures made up of a multitude of small members that tends to the shapes of Michell structures (see Fig 1.5) [35, 36]. While it is known that these structures are nearly optimal, one would want to limit the complexity of the resulting structure. Substituting $\boldsymbol{\ell}$ with $\tilde{\boldsymbol{\ell}} = [\ell_1 + s, \ell_2 + s, \ldots, \ell_{N\text{el}} + s]^T$ in the objective function of $\mathbb{P}_0$, one would penalize the appearance of small members [42]. $\tilde{\boldsymbol{\ell}}$ is called augmented member length and s the joint cost. This approach mimics the mesh-independency regularization filter of topology optimization, avoiding the inevitable apparition of structures with tiny features when a fine mesh is adopted.

2. Dorn et al. (1964), 'Automatic design of optimal structures'
12. Bendsøe et al. (2004), *Topology Optimization*
35. Michell (1904), 'The limits of economy of material in frame-structures'
36. Gilbert et al. (2003), 'Layout optimization of large-scale pin-jointed frames'
42. Parkes (1975), 'Joints in optimum frameworks'

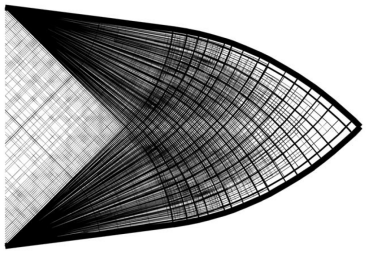

Figure 1.5: The optimal structures found by layout optimization tend at Michell-like structures, made up by a very large number of infinitesimal struts [36].

1.2 Comparison between continuous and truss discretization

In the upcoming discussion, we will be comparing the optimized structures using discrete and continuous meshes. Our primary objective in this comparison is to gain a comprehensive understanding of the application limits inherent in these two structural discretization methods. If, indeed, we identify such limitations, the aim is to discern and define them.

Since our interest in ultralight structures, we are especially interested in comparing the results of both optimization methods when dealing

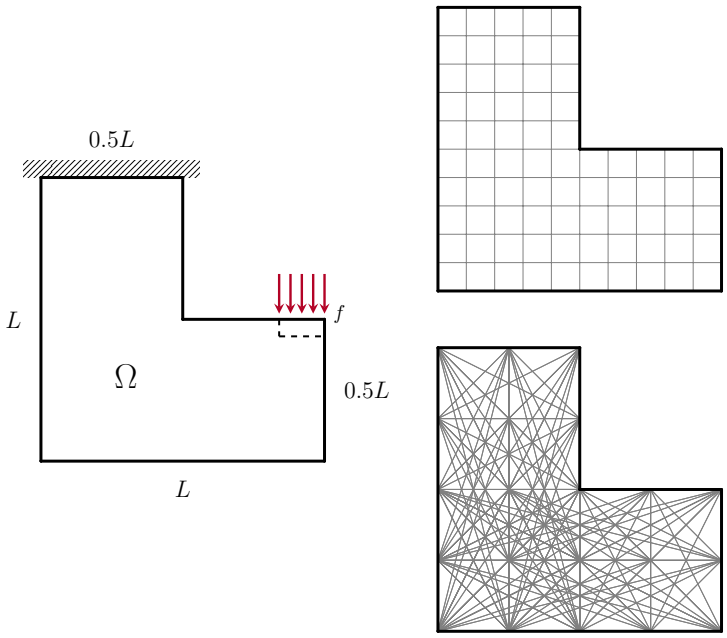

Figure 1.6: caption

with different volume fractions on a common load case. Since we can't directly control volume in our formulation, we will adjust the material properties to influence the volume fraction of the optimized structure. For this comparative analysis, we have selected three key performance metrics: the volume fraction $V_f = V/\Omega$, the structural compliance C, and the maximum material allowable σ_L. Among these, we classify stress limit as the active metric used to influence the optimization, while volume and compliance are the objective of the optimization and a passive metric, respectively. In addition to the aforementioned performance metrics, we will also track the execution time of the algorithms.

1.2.1 Definition of a common test case

The L-shape beam is one of the most used load case benchmark for stress based topology optimization [23, 24]. This choice is driven by the distinctive geometry of the problem, which generates a stress concentration, particularly at the sharp corner—a phenomenon approaching infinity. Consequently, optimized solutions often feature a large fillet, mitigating the intensity of the stress singularity. The geometric description of the test case is given in Fig. 1.6. The beam with dimensions $L \times L$ present an encastre on the top part and a load on the rigth extremity. For the continuous mesh case the load is distributed over multiple elements (5% of L) to avoid stress concentrations and the stress constraints are not evalued there. This zone is considered outside of the design domain Ω.

23. Duysinx et al. (1998), 'Topology optimization of continuum structures with local stress constraints'
24. Le et al. (2010), 'Stress-based topology optimization for continua'

To permit the discretization comparison, the structure is divided into two distinct meshes: in the continuous case, we employ a mesh consisting of 600×600 quadrilateral elements, totaling 270 000 elements,

while for the truss configuration, we employ a mesh with 33×33 nodes and a fully connected ground structure, comprising a total of 305 728 candidates.

We employ the same isotropic material and structure dimensions for the two optimization, and the complete data is resumed in Table 1.1. The value of the maximum material admissible σ_{L} is used as the parameter that influences the volume fraction of the solutions. For simplicity, all numeric values are assumed normalized and dimensionless.

Parameter	Value
E	1
ν	0.3
L	100
σ_{L}	var.

Table 1.1: Material data used for the optimizations. The value of the maximum material admissible σ_{L} is used as the parameter to generate multiple optimized topologies.

1.2.2 Numerical application

The focus of this section is to provide the numerical framework used to carry out the comparative analysis of the optimization results obtained from continuous and truss discretizations. The optimization formulations previously described have been implemented using Python.

The optimizing algorithm chosen for the continuous mesh is the Method of Moving Asymptotes (MMA) [43]. The parameter called *movelimit*[4] is set to 0.1 while the other algorithm's parameters are set to their default value. A continuation scheme for the aggressiveness of the projection parameter β is set to increase by one every 200 iterations, the number of max iteration is set to 7500, the stopping criteria is calculated as $\|r_k\|_2/\sqrt{N_e}$ on the physical densities $\overline{\overline{\rho}}$ [20], and it is set to 10^{-4}. The aggregation parameter P of the aggregation function $G^{\mathrm{L}}_{\mathrm{KS}}$ is set to 32. The numerical implementation is carried out using the NLopt Python optimization framework [44], using the sensitivity.

Formulation $\mathbb{P}_0$ represents a LP problem that can be efficiently solved by modern algorithms. In this work, we used the Python package CVXPY 1.2.2 [45] with the ECOS 2.0.7 [46] solver. As Formulation is linear, no sensitivity calculation is carried out.

The optimizations presented in this section are performed on a server equipped with an Intel® Core™ totot and 6 GB of RAM.

43. Svanberg (1987), 'The method of moving asymptotes—a new method for structural optimization'

4: More information on the implementation of the *movelimit* parameter can be found on the paper by Verbart [25]

44. Johnson (2007), *The NLopt nonlinear-optimization package*

45. Diamond et al. (2016), *CVXPY: A Python-Embedded Modeling Language for Convex Optimization*

46. Domahidi et al. (2013), 'ECOS: An SOCP solver for embedded systems'

Coninuous mesh optimization results In this section we generate multiple optimized structures with diferent volume fractions V_{f} by launching the optimization code for continuous mesh with different values of the material admissible σ_{L} spanning from 0.2 to 20.

On top of volume fraction, compliance and stress, we evaluate an additional metric propre au maillage continu called the *measure of non-discreteness* [19] to evaluate the quality of the solutions. It is defined as:

$$M_{\mathrm{nd}} = \frac{\sum_e 4\overline{\overline{\rho}}_e(1-\overline{\overline{\rho}}_e)}{n} \times 100\%, \tag{1.40}$$

where results near-zero mean a completely black and white design.

19. Sigmund (2007), 'Morphology-based black and white filters for topology optimization'

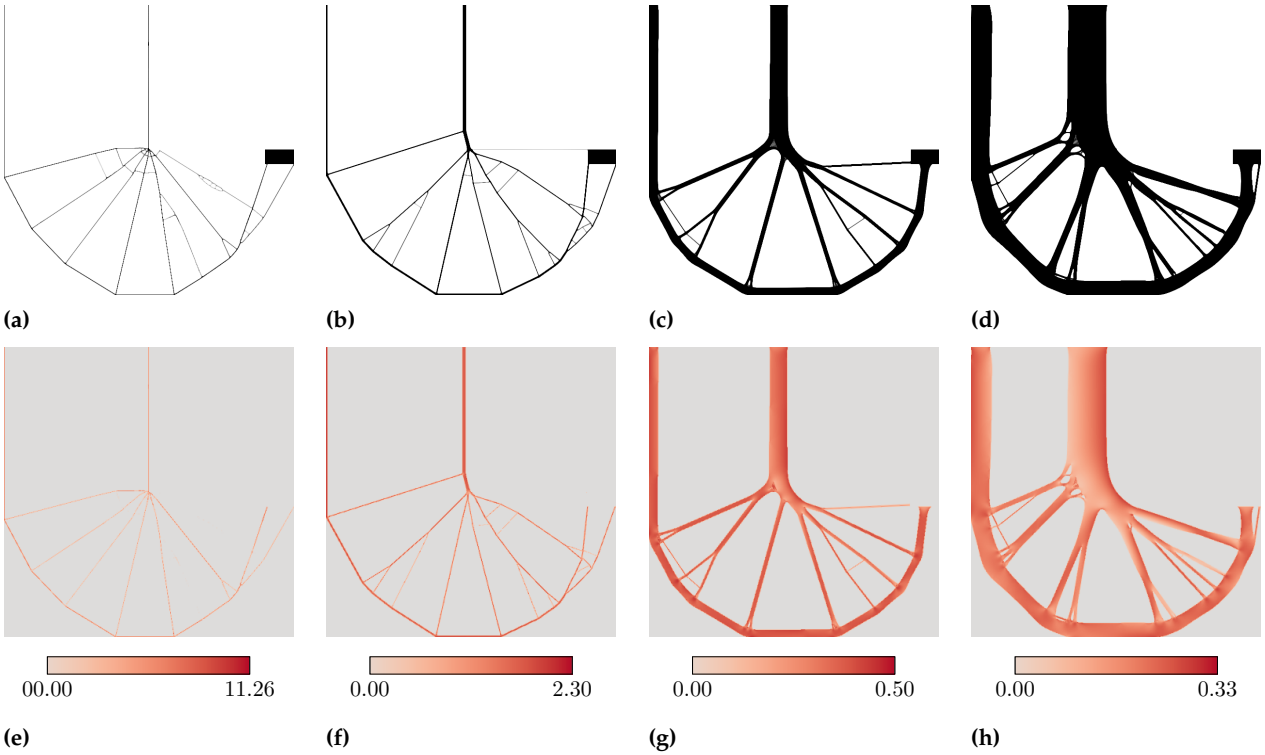

Figure 1.7: todo

The results obtained for $\sigma_L = 10.00, 2.00, 0.40$ and 0.25 are shown in Fig. 1.7. In the upper part of the figure we see the topology of the optimized structures with a clearly ascending volume fraction V_f. Interestingly, the topology of the solution remains almost unchanged, varying principally the thickness of his members. We notice the classic large fillet around the corner that alleviate the stress concentration problem. As the volume decrease, the optimized structure tend to a solution that ressemble Michell structures. In those cases we know that the topology optimization algorithm act like a method for layout of truss-like structures [6]. This effect is caused by the combination of different factors, as the regularization filter, the mesh size and the low volume fraction [47]. A summary of the numerical results is presented in Table 1.2.

6. Bendsøe et al. (1988), 'Generating optimal topologies in structural design using a homogenization method'

47. Sigmund et al. (2016), 'On the (non-)optimality of Michell structures'

In the lower part of Fig. 1.7, we plot the equivalent Von Mises stress for every element of the solution with pysical density $\overline{\overline{\rho}} > 0.5$. Multiple interesting observations can be made. First, we notice that the stress distribution is almost uniform in the structure, and it tend to the value of the material admissible σ_L – i.e. we approach a *fully stressed* structure. Even if the geometric support of the teory are different, it looks like the topology optimized structures follows the Michell criteria presented in Section 1.1.2 for optimal truss structures. Furthermore, it is observed that the maximum stress exceeds the material admissible σ_L. Aggregation methods aim to estimate the maximum value of the

σ_L	**max** σ_L	V_f	C	M_{nd}	**It.**	**Time**
20.00	23.51	1.18	6992	1.91 %	1142	8 h 11 m
10.00	11.26	1.60	3837	2.19 %	1147	7 h 55 m
8.00	8.78	1.74	2766	1.95 %	792	5 h 39 m
6.00	7.15	1.89	2243	1.81 %	806	5 h 35 m
5.00	5.81	2.17	1823	1.81 %	849	5 h 53 m
4.00	4.69	2.67	1424	2.02 %	894	6 h 12 m
3.00	3.47	3.00	1133	1.64 %	993	6 h 45 m
2.00	2.30	4.04	781	1.45 %	1189	8 h 20 m
1.00	1.18	7.28	404	1.35 %	1621	11 h 41 m
0.90	1.06	8.09	365	1.31 %	1656	11 h 36 m
0.80	0.96	8.82	332	1.21 %	1937	15 h 21 m
0.70	0.84	10.05	292	1.09 %	1827	13 h 21 m
0.60	0.73	11.80	250	1.19 %	1955	14 h 21 m
0.50	0.61	14.18	213	1.06 %	2032	15 h 39 m
0.40	0.50	18.03	170	1.08 %	2259	17 h 6 m
0.35	0.44	21.12	148	1.15 %	2421	19 h 29 m
0.30	0.38	26.21	126	1.50 %	3100	24 h 46 m
0.25	0.33	34.71	104	1.04 %	3484	27 h 39 m
0.20	0.27	48.08	77	1.26 %	7500	91 h 46 m

Table 1.2: TO

stress constraint across a group of elements. However, these aggregation methods do not perfectly align with the exact maximum value, which is a recognized limitation. To address this challenge, multiple approaches have been proposed within the aggregation framework to accurately account for the true constraint value, like using a set of active stress constraints [48], several aggregation clusters [49] or rectifier functions [50].

Looking again at Table 1.2, we notice that the optimization processes exhibit prolonged execution times, especially when dealing with extreme cases like high volume fractions. This effect is likely caused by the very fine mesh used to discretize the design domain Ω and by the sensitivity calculation by the means of the adjoint method.

As previously mentioned, our focus lies in exploring the method's limits, particularly at the boundaries. When dealing with excessively weak materials, we encounter a scenario where no solution can be attained since no distribution can simultaneously fulfill the imposed constraints. Throughout our research with this specific test case and mesh size, we did not produce any solutions with a volume fraction exceeding 50%. Although we haven't reached that scenario with σ_L set to 0.2, the calculation time and the number of iterations increase significantly, we have encountered the method's limits. The calculation time has significantly increased because the algorithm faces greater difficulty in satisfying the stress constraints. Fig. 1.8 shows the topology of the solution with $\sigma_L = 0.2$, $V_f = 48.08\%$ and over five days of optimization.

48. Bruggi et al. (2012), 'Topology optimization for minimum weight with compliance and stress constraints'

49. París et al. (2010), 'Block aggregation of stress constraints in topology optimization of structures'

50. Norato et al. (2022), 'A maximum-rectifier-function approach to stress-constrained topology optimization'

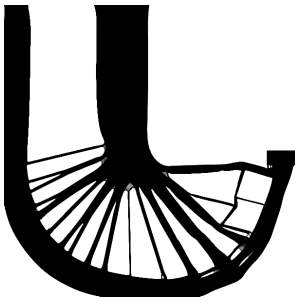

Figure 1.8: add mnd

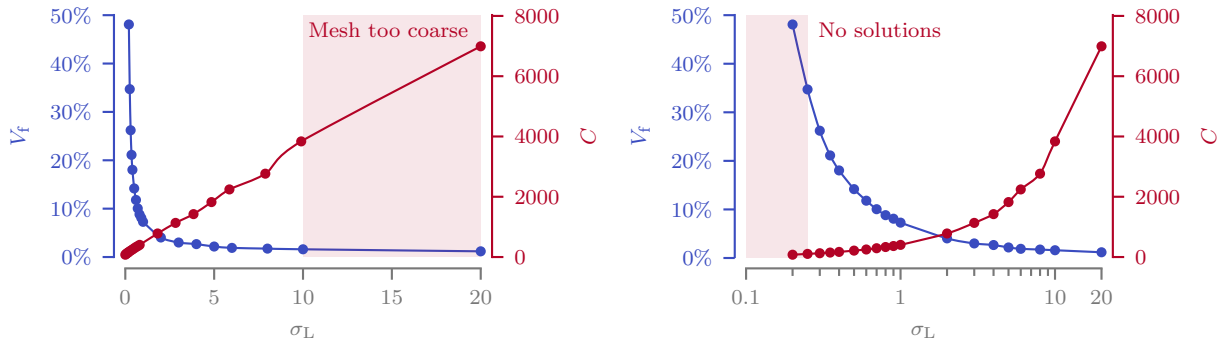

(a) **(b)**

Figure 1.10

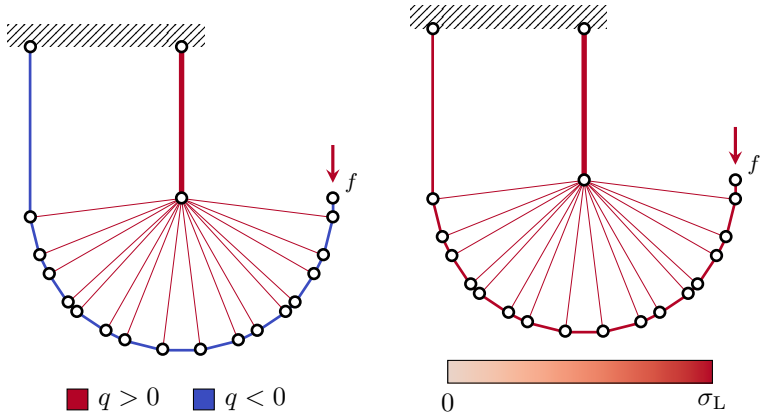

(a) **(b)**

Figure 1.11: testtesttest

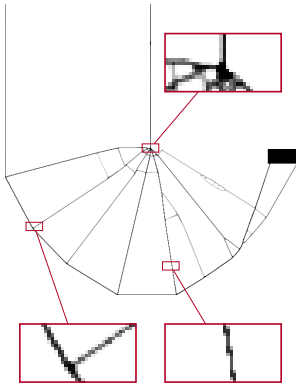

Figure 1.9: todo

Conversely, when dealing with an exceedingly strong material, the optimal scenario would demand such minimal material usage that certain sections of the structure become thinner than the width of a single element. In this case, the mesh used for discretization is too coarse to accurately represent the solution, and finer meshing becomes essential to capture the intricate details of the optimized design. Fig. 1.9 shows the limit case when $\sigma_L = 10.0$ and $V_f = 1.60\%$ pulisci grafici e tabella dai risultati fuori dai limiti

Finally, in Fig. 1.10 are the plots summarizing our findings, with the limits highlighted. To effectively show the different orders of magnitude present in the plot, we have used both linear and logarithmic scales simultaneously. It's interesting to note that the volume fraction V_f follows a hyperbolic relationship, while compliance C exhibits a linear correlation with respect to the material admissible σ_L.

Truss mesh optimization results we present here the results of the truss discretization. hre in fig the topology and the stress of the solutions for every stress limit. as formulation P0 with the L test case and simmetric stress constraints respect the michell crtiteria the solution topology is the same and it is fully stressed.

σ_L	V_f	C	Min λ	Time
50.0	0.12	23 282	111.7	1 m 6 s
20.0	0.31	9313	70.6	1 m 9 s
10.0	0.62	4656	49.9	1 m 18 s
8.0	0.78	3725	44.7	1 m 15 s
6.0	1.03	2794	38.7	1 m 10 s
5.0	1.24	2328	35.3	1 m 24 s
4.0	1.55	1863	31.6	1 m 18 s
3.0	2.07	1397	27.4	1 m 15 s
2.0	3.10	931	22.3	1 m 15 s
1.0	6.21	466	15.8	1 m 17 s
0.9	6.90	419	15.0	1 m 20 s
0.8	7.76	373	14.1	1 m 21 s
0.7	8.87	326	13.2	1 m 16 s
0.6	10.35	279	12.2	1 m 20 s
0.5	12.42	233	11.2	1 m 22 s

Table 1.3: TTO

$$PL/\sigma \tag{1.41}$$

[51] is constant

51. Lewiński et al. (1994), 'Extended exact solutions for least-weight truss layouts—Part I'

the execution time is on the order of 60 s. full results are availabe in table ..

dire che visto il test di convergenza suiulla mesh della TO prendiamo una mesh qui 33x33 ma che in realta il risutato buono ce lo abbiamo anche gia soltanto a 13x 13 con tempo di calcolo irrisorio

To explore telimit of the method we look at the boundary. in order to evaluate the quality we use a different metric segna da qualche parte la slenderness maximum minimum slenderness ratio λ (ratio between the length and the radius of gyration of the bar) of a bar is

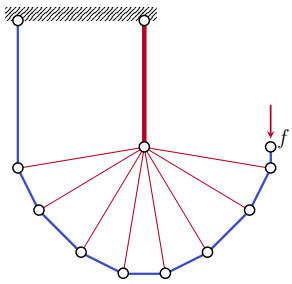

Figure 1.12: todo

the compliance is linear and the volume is hyperbolic exactly

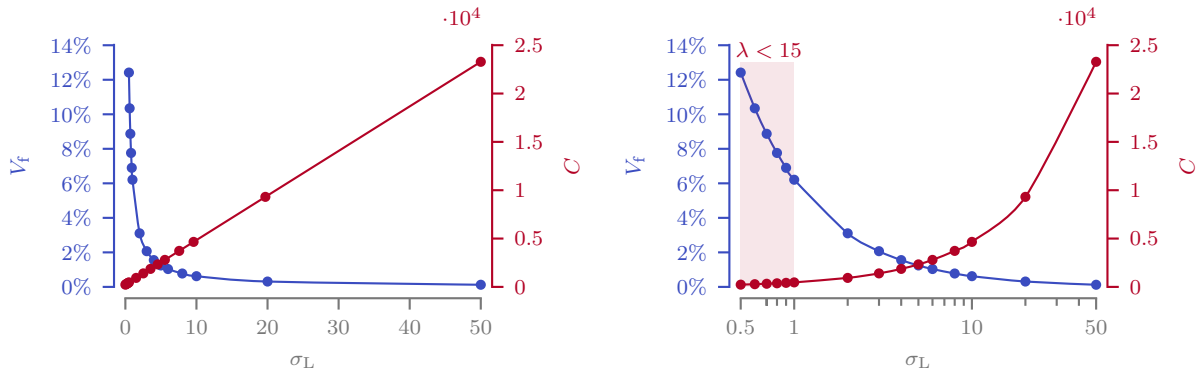

(a) **(b)**

Figure 1.13

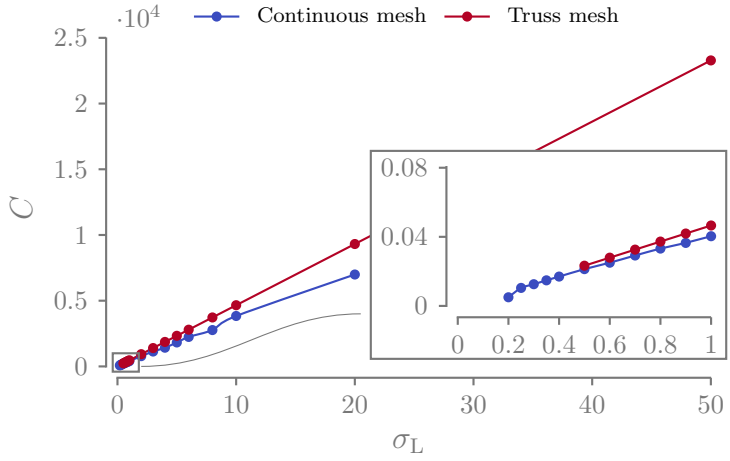

Figure 1.14: caption

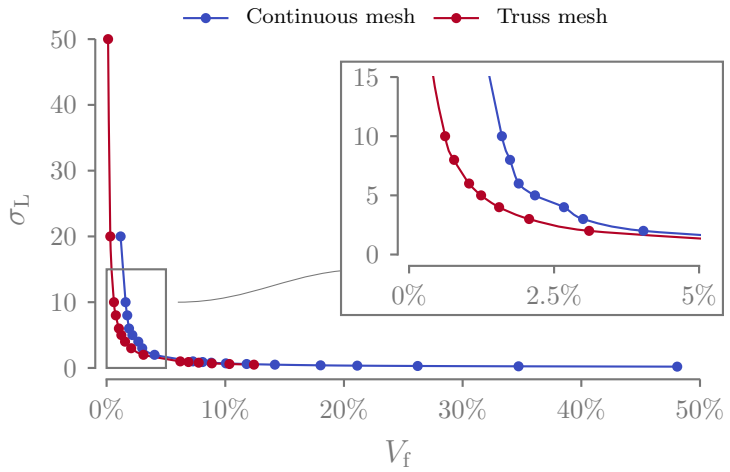

Figure 1.15: caption

1.2.3 Discussion

We present here the comparison graph of the two formulations the graphs are trimmed to their limits

Stress-compliance graph the truss is always less compliant and linear

Stress-volume graph The TO generate structures that for a given material admissible are more massive. scrivi che la differenza ad alti volumi viene dal fatto che c'é un cap allo spessore massimo nella TO

interesting that the the truss representation is the bourne inferieur de la TO for low volume fraction, while interestingly the two discretization follows the same allure for high volume fractions despite the big pysical description difference

Volume-compliance graph fai check che tutti i dati nella comparison abbiano senso e riempi i dati con il 50

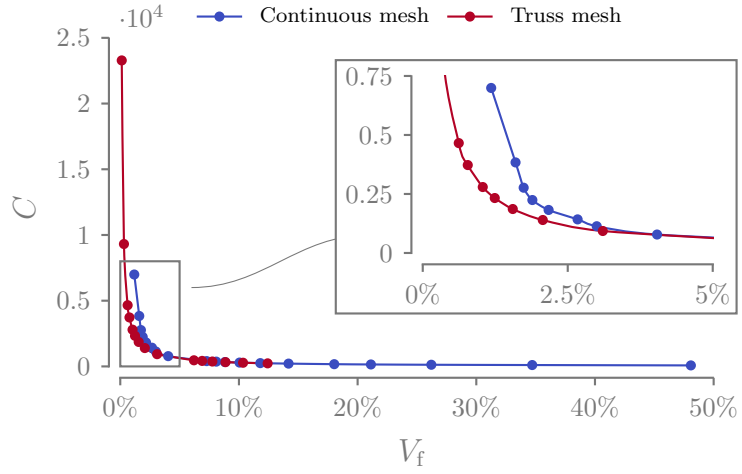

Figure 1.16: caption

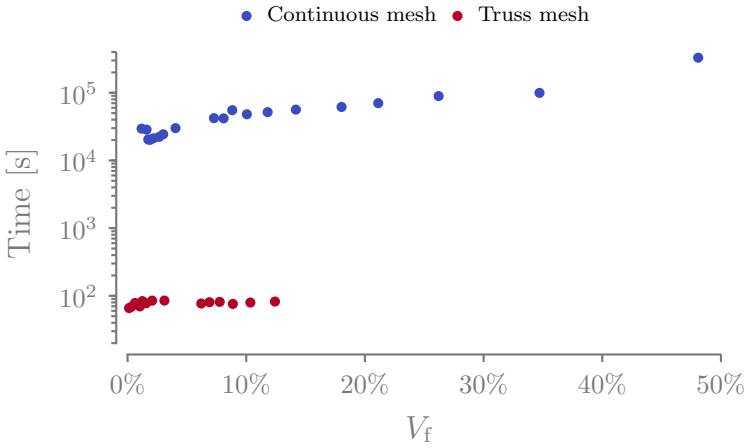

Figure 1.17: caption

finally we observe the time comparison time comparison

When stress no self adjoint SAND could be benificial however to add more constraints such as stress buckling and displacements because in that way no self adjoint

calculation time for the double of opt variables, open up the way toward sand topopt One should consider that SAND approaches usually increases the number of design variables considerably. Nevertheless, in truss topology problems this is less concerning, as the ground structure approach results in numerous cross-sectional area design variables and fewer displacement-related ones. This, however, does not hold true when dealing with a continuous mesh, where the NAND approach reduces considerably the number of design variables.

additionally interesting how the solution is not influenced by the number of nodes. expecially at low volume fration vs TO that needs more an more elements the finer we want to go

other limits of the continuous discretizations

cita l'overshoot dello stress, risolvibile ma a patto di aumentare ancora il tempo di calcolo

buckling definition is easier on truss modeled

parla del fatto che é difficile essere asimmetrico in topopt

so we select the tto

problems of the tto (open to the new chapter) in min vol the problem is linear and unexpensive to solve, but that is not always the case if we add buckling, multiload explain the problem of compatibility quick

1.3 Conclusion

"We noted that the analytical models of the isotruss and octet truss in the literature are accurate at low relative densities, but lose their accuracy for higher relative densities. Relative errors of 10% in the elastic moduli existed at all relative densities greater than approximately 2%." [52] "The methods allow for a determination of the topology of a mechanical element and give useful information on the form of the boundaries of the optimal shape. For moderately low volume fractions the lay-out of truss-like structures is predicted, but for very low volume fractions it is recommended that the traditional lay-out theory be employed, as described by Rozvany (1984)." [7]

52. Watts et al. (2019), 'Simple, accurate surrogate models of the elastic response of three-dimensional open truss micro-architectures with applications to multiscale topology design'

7. Bendsøe (1989), 'Optimal shape design as a material distribution problem'

but the performance gap has never been mesurated nor the domain of appicability. here's wy of this chapter. on the top of that these assumptions where on complaince formulations we have introduced the formulation we have run the analysis on a common load case we have compared the results we have selected the truss topology optimization BUT Open to the new chapter

Bibliography

[1] Stragiotti, Enrico et al., 'Towards manufactured lattice structures: a comparison between layout and topology optimization', *AeroBest 2021 International Conference on Multidisciplinary Design Optimization of Aerospace Systems. Book of proceedings*, Lisbon, Portugal: ECCOMAS, July 2021, pp. 229–244. cited on page 1

[2] Dorn, W. S., Gomory, Ralph E., and Greenberg, H., 'Automatic design of optimal structures', *J. Mécanique* (1964). cited on pages 1, 12, 13

[3] Chan, H. S. Y., 'Optimum structural design and linear programming', *College of Aeronautics Report Aero 175* (1964), Publisher: College of Aeronautics Cranfield. cited on pages 1, 12

[4] Hemp, W. S., *Optimum Structures*. Clarendon Press, 1973, Google-Books-ID: cJhpAAAAMAAJ. cited on pages 1, 11, 12

[5] Sankaranarayanan, S., Haftka, Raphael T., and Kapania, Rakesh K., 'Truss topology optimization with simultaneous analysis and design', *AIAA Journal* 32.2 (Feb. 1994), pp. 420–424. DOI: 10.2514/3.12000 cited on page 1

[6] Bendsøe, Martin Philip and Kikuchi, Noboru, 'Generating optimal topologies in structural design using a homogenization method', *Computer Methods in Applied Mechanics and Engineering* 71.2 (Nov. 1988), pp. 197–224. DOI: 10.1016/0045-7825(88)90086-2 cited on pages 1, 16

[7] Bendsøe, M. P., 'Optimal shape design as a material distribution problem', *Structural optimization* 1.4 (Dec. 1989), pp. 193–202. DOI: 10.1007/BF01650949 cited on pages 1, 3, 22

[8] Sigmund, Ole, 'Materials with prescribed constitutive parameters: An inverse homogenization problem', *International Journal of Solids and Structures* 31.17 (Sept. 1994), pp. 2313–2329. DOI: 10.1016/0020-7683(94)90154-6 cited on page 1

[9] Zhang, Weihong and Sun, Shiping, 'Scale-related topology optimization of cellular materials and structures', *International Journal for Numerical Methods in Engineering* 68.9 (2006), _eprint: https://onlinelibrary.wiley.com/doi/pdf/10.1002/nme.1743, pp. 993–1011. DOI: 10.1002/nme.1743 cited on page 1

[10] Tortorelli, D. A. and Michaleris, P., 'Design sensitivity analysis: Overview and review', *Inverse Problems in Engineering* 1.1 (Oct. 1994), Publisher: Taylor & Francis _eprint: https://doi.org/10.1080/174159794088027573, pp. 71–105. DOI: 10.1080/174159794088027573 cited on page 2

[11] Martins, J.R.R.A. and Ning, A., *Engineering Design Optimization*. Cambridge University Press, 2021. cited on pages 2, 10

cited on pages 2, 10, 13 [12] Bendsøe, Martin P. and Sigmund, Ole, *Topology Optimization*. Berlin, Heidelberg: Springer Berlin Heidelberg, 2004.

cited on pages 3, 4 [13] Wang, Fengwen, Lazarov, Boyan Stefanov, and Sigmund, Ole, 'On projection methods, convergence and robust formulations in topology optimization', *Structural and Multidisciplinary Optimization* 43.6 (June 2011), pp. 767–784.
DOI: 10.1007/s00158-010-0602-y

cited on page 3 [14] Bendsøe, M. P. and Sigmund, O., 'Material interpolation schemes in topology optimization', *Archive of Applied Mechanics* 69.9 (Nov. 1999), pp. 635–654.
DOI: 10.1007/s004190050248

cited on page 3 [15] Hashin, Z. and Shtrikman, S., 'A variational approach to the theory of the elastic behaviour of multiphase materials', *Journal of the Mechanics and Physics of Solids* 11.2 (Mar. 1963), pp. 127–140.
DOI: 10.1016/0022-5096(63)90060-7

cited on page 3 [16] Díaz, A. and Sigmund, O., 'Checkerboard patterns in layout optimization', *Structural optimization* 10.1 (Aug. 1995), pp. 40–45.
DOI: 10.1007/BF01743693

cited on pages 3, 4 [17] Sigmund, Ole, 'Design of Material Structures using Topology Optimization', PhD thesis, Technical University of Denmark, DK-2800 Lyngby, 1994.

cited on pages 3, 4 [18] Sigmund, Ole, 'On the Design of Compliant Mechanisms Using Topology Optimization', *Mechanics of Structures and Machines* 25.4 (Jan. 1997), pp. 493–524.
DOI: 10.1080/08905459708945415

cited on pages 4, 15 [19] Sigmund, Ole, 'Morphology-based black and white filters for topology optimization', *Structural and Multidisciplinary Optimization* 33.4 (Apr. 2007), pp. 401–424.
DOI: 10.1007/s00158-006-0087-x

cited on pages 4, 15 [20] Ferrari, Federico and Sigmund, Ole, 'A new generation 99 line Matlab code for compliance topology optimization and its extension to 3D', *Structural and Multidisciplinary Optimization* 62.4 (Oct. 2020), pp. 2211–2228.
DOI: 10.1007/s00158-020-02629-w

cited on page 5 [21] Achtziger, Wolfgang and Kanzow, Christian, 'Mathematical programs with vanishing constraints: optimality conditions and constraint qualifications', *Mathematical Programming* 114.1 (July 2008), pp. 69–99.
DOI: 10.1007/s10107-006-0083-3

cited on page 5 [22] Cheng, Gengdong and Jiang, Zheng, 'Study on Topology Optimization with Stress Constraints', *Engineering Optimization* 20.2 (Nov. 1992), pp. 129–148.
DOI: 10.1080/03052159208941276

[23] Duysinx, P. and Bendsøe, M. P., 'Topology optimization of continuum structures with local stress constraints', *International Journal for Numerical Methods in Engineering* 43.8 (1998), _eprint: https://onlinelibrary.wiley.com/doi/pdf/10.1002/%28SICI%291097-0207%2819981230%2943%3A8%3C1453%3A%3AAID-NME480%3E3.0.CO%3B2-2, pp. 1453–1478.
DOI: 10.1002/(SICI)1097-0207(19981230)43:8<1453::AID-NME480>3.0.CO;2-2 cited on pages 6, 14

[24] Le, Chau et al., 'Stress-based topology optimization for continua', *Structural and Multidisciplinary Optimization* 41.4 (Apr. 2010), pp. 605–620.
DOI: 10.1007/s00158-009-0440-y cited on pages 6, 7, 14

[25] Verbart, Alexander, Langelaar, Matthijs, and Keulen, Fred van, 'A unified aggregation and relaxation approach for stress-constrained topology optimization', *Structural and Multidisciplinary Optimization* 55.2 (Feb. 2017), pp. 663–679.
DOI: 10.1007/s00158-016-1524-0 cited on pages 6, 7, 15

[26] Holmberg, Erik, Torstenfelt, Bo, and Klarbring, Anders, 'Stress constrained topology optimization', *Structural and Multidisciplinary Optimization* 48.1 (2013), pp. 33–47.
DOI: 10.1007/s00158-012-0880-7 cited on page 7

[27] Silva, Gustavo Assis da, Beck, André Teófilo, and Sigmund, Ole, 'Stress-constrained topology optimization considering uniform manufacturing uncertainties', *Computer Methods in Applied Mechanics and Engineering* 344 (Feb. 2019), pp. 512–537.
DOI: 10.1016/j.cma.2018.10.020 cited on page 7

[28] Rozvany, G.I.N., 'On design-dependent constraints and singular topologies', *Structural and Multidisciplinary Optimization* 21.2 (Apr. 2001), pp. 164–172.
DOI: 10.1007/s001580050181 cited on page 7

[29] Stolpe, Mathias, 'On Models and Methods for Global Optimization of Structural Topology', Publisher: Matematik, PhD thesis, 2003. cited on page 7

[30] Sved, G. and Ginos, Z., 'Structural optimization under multiple loading', *International Journal of Mechanical Sciences* 10.10 (Oct. 1968), pp. 803–805.
DOI: 10.1016/0020-7403(68)90021-0 cited on page 7

[31] Cheng, G. D. and Guo, X., 'ε-relaxed approach in structural topology optimization', *Structural optimization* 13.4 (June 1997), pp. 258–266.
DOI: 10.1007/BF01197454 cited on page 7

[32] Silva, Gustavo Assis da et al., 'Local versus global stress constraint strategies in topology optimization: A comparative study', *International Journal for Numerical Methods in Engineering* cited on page 7

122.21 (2021), _eprint: https://onlinelibrary.wiley.com/doi/pdf/10.1002/nme.67
pp. 6003–6036.
DOI: 10.1002/nme.6781

cited on page 8 [33] Kreisselmeier, G. and Steinhauser, R., 'Systematic Control Design by Optimizing a Vector Performance Index', *IFAC Proceedings Volumes*, IFAC Symposium on computer Aided Design of Control Systems, Zurich, Switzerland, 29-31 August 12.7 (Sept. 1979), pp. 113–117.
DOI: 10.1016/S1474-6670(17)65584-8

cited on page 11 [34] Maxwell, J. Clerk, 'I.—On Reciprocal Figures, Frames, and Diagrams of Forces', *Earth and Environmental Science Transactions of The Royal Society of Edinburgh* 26.1 (1870), Publisher: Royal Society of Edinburgh Scotland Foundation, pp. 1–40.
DOI: 10.1017/S0080456800026351

cited on pages 11, 13 [35] Michell, A. G. M., 'The limits of economy of material in frame-structures', *The London, Edinburgh, and Dublin Philosophical Magazine and Journal of Science* 8.47 (Nov. 1904), Publisher: Taylor & Francis _eprint: https://doi.org/10.1080/14786440409463229, pp. 589–597.
DOI: 10.1080/14786440409463229

cited on pages 12, 13 [36] Gilbert, Matthew and Tyas, Andrew, 'Layout optimization of large-scale pin-jointed frames', *Engineering Computations* 20.8 (Dec. 2003), pp. 1044–1064.
DOI: 10.1108/02644400310503017

cited on page 12 [37] Pedersen, Pauli, 'Optimal Joint Positions for Space Trusses', *Journal of the Structural Division* 99.12 (Dec. 1973), Publisher: American Society of Civil Engineers, pp. 2459–2476.
DOI: 10.1061/JSDEAG.0003669

cited on page 12 [38] Achtziger, Wolfgang, 'On simultaneous optimization of truss geometry and topology', *Structural and Multidisciplinary Optimization* 33.4 (Apr. 2007), pp. 285–304.
DOI: 10.1007/s00158-006-0092-0

cited on page 12 [39] Descamps, Benoît and Filomeno Coelho, Rajan, 'A lower-bound formulation for the geometry and topology optimization of truss structures under multiple loading', *Structural and Multidisciplinary Optimization* 48.1 (July 2013), pp. 49–58.
DOI: 10.1007/s00158-012-0876-3

cited on page 12 [40] He, L. and Gilbert, M., 'Rationalization of trusses generated via layout optimization', *Structural and Multidisciplinary Optimization* 52.4 (Oct. 2015), pp. 677–694.
DOI: 10.1007/s00158-015-1260-x

cited on page 12 [41] Lu, Hongjia and Xie, Yi Min, 'Reducing the number of different members in truss layout optimization', *Structural and Multidisciplinary Optimization* 66.3 (Feb. 2023), p. 52.
DOI: 10.1007/s00158-023-03514-y

[42] Parkes, E.W., 'Joints in optimum frameworks', *International Journal of Solids and Structures* 11.9 (Sept. 1975), pp. 1017–1022. DOI: 10.1016/0020-7683(75)90044-X cited on page 13

[43] Svanberg, Krister, 'The method of moving asymptotes—a new method for structural optimization', *International Journal for Numerical Methods in Engineering* 24.2 (1987), pp. 359–373. DOI: https://doi.org/10.1002/nme.1620240207 cited on page 15

[44] Johnson, Steven G., *The NLopt nonlinear-optimization package*, https://github.com/stevengj/nlopt, 2007. cited on page 15

[45] Diamond, Steven and Boyd, Stephen, *CVXPY: A Python-Embedded Modeling Language for Convex Optimization*, 2016. cited on page 15

[46] Domahidi, Alexander, Chu, Eric, and Boyd, Stephen, 'ECOS: An SOCP solver for embedded systems', *2013 European Control Conference (ECC)*, Zurich: IEEE, July 2013, pp. 3071–3076. DOI: 10.23919/ECC.2013.6669541 cited on page 15

[47] Sigmund, Ole, Aage, Niels, and Andreassen, Erik, 'On the (non-)optimality of Michell structures', *Structural and Multidisciplinary Optimization* 54.2 (Aug. 2016), pp. 361–373. DOI: 10.1007/s00158-016-1420-7 cited on page 16

[48] Bruggi, Matteo and Duysinx, Pierre, 'Topology optimization for minimum weight with compliance and stress constraints', *Structural and Multidisciplinary Optimization* 46.3 (Sept. 2012), pp. 369–384. DOI: 10.1007/s00158-012-0759-7 cited on page 17

[49] París, J. et al., 'Block aggregation of stress constraints in topology optimization of structures', *Advances in Engineering Software*, Advances in optimum engineering design 41.3 (Mar. 2010), pp. 433–441. DOI: 10.1016/j.advengsoft.2009.03.006 cited on page 17

[50] Norato, Julián A. et al., 'A maximum-rectifier-function approach to stress-constrained topology optimization', *Structural and Multidisciplinary Optimization* 65.10 (Sept. 2022), p. 286. DOI: 10.1007/s00158-022-03357-z cited on page 17

[51] Lewiński, T., Zhou, M., and Rozvany, G. I. N., 'Extended exact solutions for least-weight truss layouts—Part I: Cantilever with a horizontal axis of symmetry', *International Journal of Mechanical Sciences* 36.5 (1994), pp. 375–398. DOI: 10.1016/0020-7403(94)90043-4 cited on page 19

[52] Watts, Seth et al., 'Simple, accurate surrogate models of the elastic response of three-dimensional open truss micro-architectures with applications to multiscale topology design', *Structural and Multidisciplinary Optimization* 60.5 (Nov. 2019), pp. 1887–1920. DOI: 10.1007/s00158-019-02297-5 cited on page 22